Influence of porosity on the high temperature oxidation of a SiC-reinforced Si_3N_4 ceramic composite

H. F. LÓPEZ, W. PHOOMIPHAKDEEPHAN
Materials Department, CEAS, University of Wisconsin-Milwaukee, P.O. Box 784, Milwaukee WI 53201, USA
E-mail: hlopez@uwm.edu

In this work the oxidation kinetics of a porous (21.5% porosity) nitride bonded silicon carbide containing 20% SiC was investigated in the temperature range of 1100–1400 °C. Two oxidation stages were found which corresponded to (i) a rapid parabolic oxidation rate during short term oxidation exposure (0–10 hours), and (ii) a parabolic scale growth after some exposure time. During short term oxidation a continuous oxide film developed, but it was unable to block internal oxidation at the pore channels. An experimental activation energy of 55 kJ/mol was obtained which was attributed to intially rapid external and internal oxidation through the open pore network. After 1–10 hours depending on the actual temperature, closure of the surface pores through oxidation lead to a transition where a continuous SiO_2 scale grew on the outer sample surface through diffusion. An activation energy of 132 kJ/mol was associated with this parabolic growth suggesting that inward oxygen diffusion through the SiO_2 scale was rate limiting. Metallographic observations indicated severe cracking of the scale developed. This was attributed to the relatively large shrinkage (≈1%) associated with the β–α cristobalite transformation occurring at temperatures below 250 °C. Moreover, X-ray diffraction indicated the presence of cristobalite and tridymite, but it was unable to identify a discontinuous phase developed beneath the SiO_2 scale during oxidation.

1. Introduction

Silicon based ceramics such as Si_3N_4 and SiC are leading candidates as structural materials in the development of advanced heat engines and heat recovery systems. Their relatively high temperature strength, low thermal expansion coefficients, and moderate thermal conductivities result in excellent transient thermal shock resistance [1, 2]. Furthermore, Si_3N_4, and SiC are considered to posses the highest oxidation resistance among the non-oxide structural ceramics [3, 4]. Since the major limitation in the widespread use of Si_3N_4 and SiC as structural materials is their relative brittlenes, fracture toughness improvements can be achieved through the use of reinforcements [5, 6]. Nevertheless, in Si_3N_4 reinforced with SiC, the high temperature strength is not significantly improved and in some cases it can be below that corresponding to monolithic Si_3N_4 [6–9].

Monolithic SiC and Si_3N_4 are inherently unstable in high temperature air giving rise to an adherent SiO_2 protective film. As a result, these ceramic materials exhibit relatively high oxidation resistances since SiO_2 possesses the lowest permeability to oxygen of all the common oxides [1, 2]. Moreover, in pure Si_3N_4 the oxide scale consists of two layers, an inner oxynitride (Si_2N_2O) layer and an external SiO_2 film [2]. In SiC an oxycarbide layer may also form in addition to the SiO_2 film, but there is limited experimental evidence for its presence [1]. In order to understand the basic oxidation mechanisms that take place in Si-based ceramics, pure Si has been used as the reference material for fundamental studies on oxidation kinetics [10, 11]. In particular, Deal and Grove [11], found three distinct steps (a) gaseous oxidant transfer to the external oxide film surface, (b) diffusion through the oxide film, and (c) oxidation reaction at the Si/SiO_2 interface. Moreover, Deal and Grove found that scale growth was parabolic after long term high temperature exposures, where diffusion of the oxidizing species through the SiO_2 scale is the rate limiting step. Nevertheless, short term oxidation follows a linear rate law probably due to interface or diffusion control and strain effects in the oxide film [11, 12].

In the case of SiC, the potential rate controlling mechanisms consist of (a) inward diffusion of oxygen, (b) outward diffusion of CO through the SiO_2 scale, and (c) interfacial reaction control at the SiO_2/SiC interface [13]. In general, it has been found that below 1350°C, the activation energies for the oxidation of SiC are similar to those corresponding to pure Si [13]. However,

above 1350°C, increasing activation energies are found which in turn indicate a combination of inward ionic oxygen transport plus molecular oxygen diffusion [14]. The possibility of outward diffusion of CO as a rate limiting step is not supported by the experimental outcome. Zheng *et al*. [15] found the lack of a carbon gradient across the SiO_2 scale suggesting rapid outward transport of CO. Alternatively, Luthra [16], has suggested a mixed control mechanism in which both oxygen and CO diffusion mixed with the interfacial reaction become rate controlling. In Si_3N_4 the oxidation mechanisms become more complex when compared with pure Si or SiC. In general, it has been found that Si_3N_4 exhibits lower oxidation rates than either Si or SiC below 1400°C. Also, above 1400°C after relatively large exposure times, the oxidation rates become somewhat similar to either Si or SiC [1–4]. Moreover, scale growth is made up of a duplex SiO_2/Si_2N_2O scale. This in turn suggests that during oxidation, inward oxygen diffusion through SiO_2 is followed by reaction at the SiO_2/Si_2N_2O interface to promote scale growth. Accordingly, the SiO_2 scale growth occurs in preference to the Si_2N_2O scale. Moreover, not all of the oxygen is consumed by the oxidation reaction at this interface, but a fraction of oxygen continues to inwardly diffuse until the Si_2N_2O/Si_3N_4 inteface is reached where Si_2N_2O scale growth is expected to occur. Hence, simultaneous growth of both SiO_2 and Si_2N_2O scales occurs and has been reported in the literature [1, 2]. In addition, parabolic scale growth has been observed in this system with the published data supporting inward diffusion of molecular oxygen as the rate limiting step [1–4]. In particular, the activation energies for oxidation of Si_3N_4 indicate that inward oxygen diffusion through the Si_2N_2O scale is the rate controlling mechanism due to its inherently low oxygen permeability and high activation energy [10].

1.1. Impurity effects

The impurities present in silica based ceramics might promote the crystallization of amorphous SiO_2. Costello and Tressler [17] have found a reduction in the oxidation reaction rates as a result of crystallization of the oxide scale since oxygen transport through the cristobalite phase is slower than for amorphous SiO_2. The exact nature of the crystallization process is strongly influenced by the manufacturing process. Hence, depending on the nature of the impurities/additives, the oxidation behavior will be drastically affected. In the case of B and C sintering aids, oxidation rates higher than those corresponding to pure SiC have been found [18, 19]. In addition, densification aids have a more dramatic effect. Refractory oxides when used as additives such as MgO, Al_2O_3 and Y_2O_3 tend to migrate to the SiO_2 scale and form a corresponding silicate. Initially these additives are present as grain boundary (gb) silicate glass. Moreover, the presence of an initially pure SiO_2 scale gives rise to a transition metal concentration gradient which drives the metal cations to diffuse into the glassy phase [9, 20]. This is followed by the formation of silicate phases due to the available free energy of the system. Hence, in this case oxidation might be controlled by the outward migration of magnesium or yttrium cations along the gb phase. In general the presence of additives might lead to higher oxidation rates, as well as to a deviation from parabolic oxidation behavior [21].

1.2. Moist environments

The oxidation behavior of silica based materials is strongly influenced by the presence of a moist environment. In particular, Deal and Grove [11] have found that Si oxidizes faster in wet than in dry oxygen. This phenomenon is attributed to the relatively high solubility of water in SiO_2 since it acts as the primary oxidizing species (H_2O vs O_2). Moreover, the oxidation kinetics exhibits a linear trend indicating that the interfacial reaction between H_2O and Si becomes the rate limiting factor [22]. In SiC, water accelerates the oxidation rate. Jorgenson *et al*. [23] found that the oxidation rate of SiC powders in moist environments is proportional to the partial water pressure. Alternatively, oxidation of Si_3N_4 in moist H_2O/O_2, exhibits a complex dependence on the partial water pressure. Accordingly, it is suggested that the water effects on the oxidation of Si_3N_4 are due to the product gases (NH_3 and NO) involved in the oxidation reactions which block the outward diffusion path [24].

1.3. Oxidation of porous ceramic composites

The introduction of additives and impurities through manufacturing in order to produce reinforced Si-based composites might affect the resultant oxidation behavior. In particular, it is likely that the resultant SiO_2 protective scale will not be able to develop a truly continuous film, which will avoid exposing the composite material to oxygen penetration through the inherent pore channels. In reaction-sintered Si_3N_4, the degree of internal oxidation is apparently controlled by the radius of the pore channels [8, 25, 26]. In particular, when the transport rate of oxygen into narrow channels is lower than that corresponding to the reaction with Si_3N_4, the end result is the formation of SiO_2 at the channel mouths [26]. This in turn leads to pore closure and the reduction in mass gain through oxidation at elevated temperatures. Moreover, oxidation of the porous Si_3N_4 is manifest as a diffusion controlled two stage process. During the first stage, linear oxidation is found for a short period and it is followed by a transition to parabolic scale growth [25]. Accordingly, the overall oxidation reaction of reaction bonded silicon nitride has been described by an asymptotic equation [26]. Moreover, the cation additives or impurities such as Mg, Ca, Fe and Al, etc, might modify the resultant silicate phases which in turn will result in a decrease in the SiO_2 viscosity, thus raising the oxidation rate. Alternatively, impurity removal through the development of a driving force for the outward diffusion of grain boundary silicate cations will in turn tend to concentrate the impurities in the oxidation surface [1, 27]. This results in improved high temperature strength of the material, as long as the scale formed is removed [9]. When SiC is used as a reinforcement, additional degradation reactions between the matrix and the reinforcement have

TABLE I Chemical composition of NBSC in the as-received condition (wt %)

SiC	Si_3N_4	Fe_2O_3	SiO_2	C	Al_2O_3	Ca	Other
27.00	68.50	1.90	1.00	0.90	0.40	0.27	0.03

to be considered. In SiC reinforced alumina, oxidation of the SiC reinforcement and its subsequent interaction with the alumina matrix leads to the development of mullite and glassy phases during the oxidation process [28–30]. In addition, it has been found that the rate of scale thickening is predominantly parabolic, with the parabolic constant decreasing for higher volume fractions of SiC. Since it is desirable to establish the high temperature performance of advanced ceramics, the present work looks at the thermal oxidation properties of a nitride bonded silicon carbide (NBSC) ceramic composite.

2. Experimental

The material employed in this work consisted of a 1.3 cm diameter nitride bonded silicon carbide rod supplied by Ceramic Systems Inc. Table I gives the NBSC composition and porosity level as well as the relative amounts of the major impurities (Fe_2O_3, Al_2O_3, SiO_2 and Ca). In addition, the properties of the NBSC in the as-received condition are given in Table II. Cylindrical specimens of 0.25 cm in thickness were exposed to still air under dry conditions in an open ended furnace between 1100 and 1400 °C for 1–60 hours. Weight changes were systematically measured in a highly sensitive microbalance as a function of time and temperature. Measurements of weight gain through oxidation were related to an apparent constant sample area given in terms of the sample diameter and thickness. In addition, scanning electron microscopy (SEM) was used to investigate the morphological changes occurring in the scale regions whereas X-ray diffraction was used for determinations of the oxide phases present.

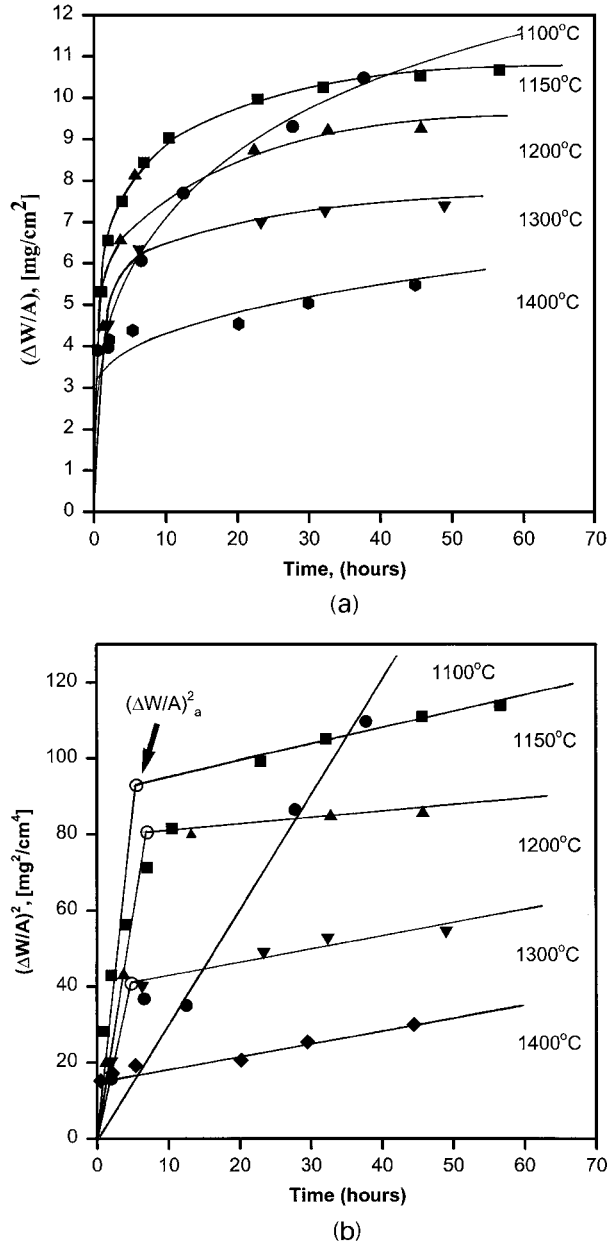

Figure 1 (a) Mass gain per unit area ($\Delta W/A$) versus time, and (b) $(\Delta W/A)^2$ versus time plots at various temperatures for the high temperature air oxidation of NBSC.

3. Results

3.1. Reaction rates

Oxidation studies carried out in the as-received NBSC as a function of time in the temperature range of 1100–1400 °C are plotted in Fig. 1a as mass gain per unit area exposed ($\Delta W/A$) versus time (t). From this figure it is shown that at 1100°C the oxidation process exhibits a parabolic trend typical of diffusion controlled processes. Nevertheless, at temperatures above 1100°C, the oxidation process exhibited two distinct stages. The initial stage of oxidation (stage I) was characterized by the rapid development of a continuous oxide film on the exposed surface, as well as within the surface interconnected sample porosity. During this stage the variations in mass ($\Delta W/A$) with time were essentially parabolic in nature. A transition to a second stage of oxidation (stage II), was found were the oxidation rates were drastically reduced, but they tended to increase

TABLE II Properties of nitride bonded silicon carbide in the as-received condition

Density (g/cm^3)	Porosity %	Hardness 45 N scale	Grain Size μm	Flexural Strength (MPa)	Poisson's Ratio	Elasticity Modulus (GPa)	Max T in Air (°C)
2.50	21.50	60–75	0.75 Si_3N_4 50–500 SiC	102 (R.T.) 115 (1000°C)	0.25	16.00	1475.00

TABLE III Apparent mass gain per unit area $(\Delta W/A)_a$, and characteristic times t_c for the transition from linear to parabolic oxidation in the porous NBSC as a function of temperature

$(\Delta W/A)_a^2$ (mg^2/cm^4)	T (°C)	t_c (hours)
93.6	1150.00	9.1
83.12	1200.00	7.70
97.60	1250.00	7.00
50.00	1300.00	7.8
49.20	1340.00	2.70
17.20	1400.00	0.90

with temperature. These two stages can be clearly distinguished by plotting $(\Delta W/A)^2$ versus t as shown in Fig. 1b. This figure shows that there is an apparent transition between two parabolic stages of scale growth. Accordingly, an apparent value of $(\Delta W/A)_a^2$, set by the intersection of the lines corresponding to each of the oxidation stages has been used arbitrarily to describe the effect of temperature on this transition. Table III gives the relative magnitudes of $(\Delta W/A)_a^2$ and corresponding times as a function of temperature. From this table it can be observed that as the temperature is increased, the transition from one to another parabolic oxidation regimes occurs at shorter times and smaller amounts of mass gain. In addition, apparent mass gain constants (k_m) were determined from the relative slopes of $(\Delta W/A)^2 - t$ plots (oxidation stages I and II, Fig. 1a, b). Fig. 2a, b are Arrhenius plots of $\ln k_m$ vs $1/T$ for the exhibited parabolic oxidation regimes I and II, respectively. From these figures, an activation energy of 55 kJ was found to correspond to the initial rapid oxidation stage I, whereas an activation energy of 132 kJ was associated with the stage II of parabolic scale growth.

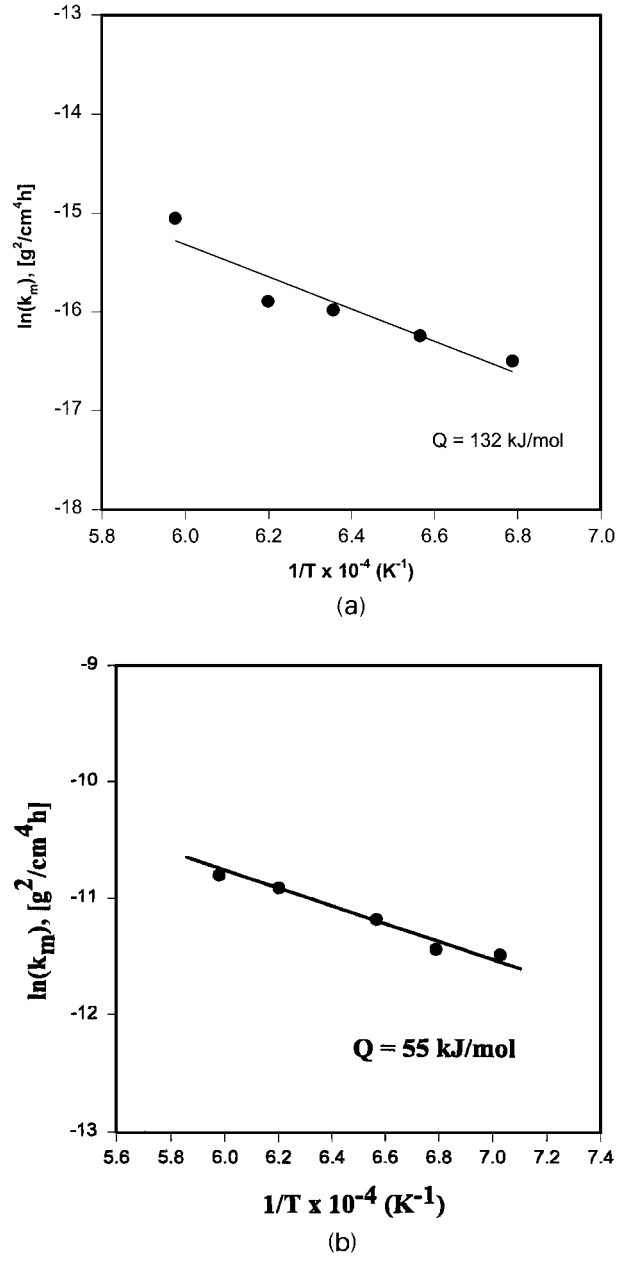

Figure 2 Arrhenius plots based on (a) parabolic mass constants (k_m) for the second stage of air oxidation, and (b) for the initial oxidation stage of NBSC.

3.2. Scale product

Although the expected scale is SiO_2 in an amorphous or crystalline condition (cristobalite), the actual scale properties are strongly influenced by the NBSC composition, type and level of impurities, and porosity level. Fig. 3a shows the distribution and morphology of SiC and Si_3N_4 phases of the NBSC in the as received condition, whereas Fig. 3b is an X-ray diffractogram of the ceramic cross section. In particular, notice from this figure that SiC particles are relatively large (i.e. 50–500 μm, Table II), whereas Si_3N_4 grains are roughly 0.75 μm in size. During short term oxidation exposure to air (<10 hours) the scales developed were continuous covering the outer sample surface and the interconnected porosity present preferentially on the Si_3N_4 phase as shown in Fig. 4a, b. Notice from figures that during stage I, even though oxidation provides a continuous film, the film is not able to prevent oxygen transport into the open pore channel network. Hence, external and internal oxidation are active until the existing channel network is sealed from the external environment through further oxidation. This transition is associated with the development of a continuous scale on the external surface (see Table III) as shown in Fig. 5a–d. In addition, it was found that the resultant continuous scale was severely cracked as shown in Fig. 5. Moreover, a discontinuous second phase subscale was clearly evidenced in specimens oxidized at all the oxidation temperatures once a continous scale was formed (Fig. 5a–d). However, it was not possible to establish the exact composition of this phase. Fig. 6 shows the presence of blisters at the air/scale interface suggesting outward permeation of possible product gases such as N_2 and CO. The appearance of gas blisters on the scale indicates that at the higher temperatures the oxide acts as a low viscosity film and fills the surface pores to generate smooth surfaces.

Measurements of scale thickness as a function of time and temperature did not provide a consistent trend due to the inhomogeneous nature of the local oxidation processes and the local differences as a result of porosity and surface irregularities. Fig. 7a, b are SEM micrographs of cross sections showing the penetration

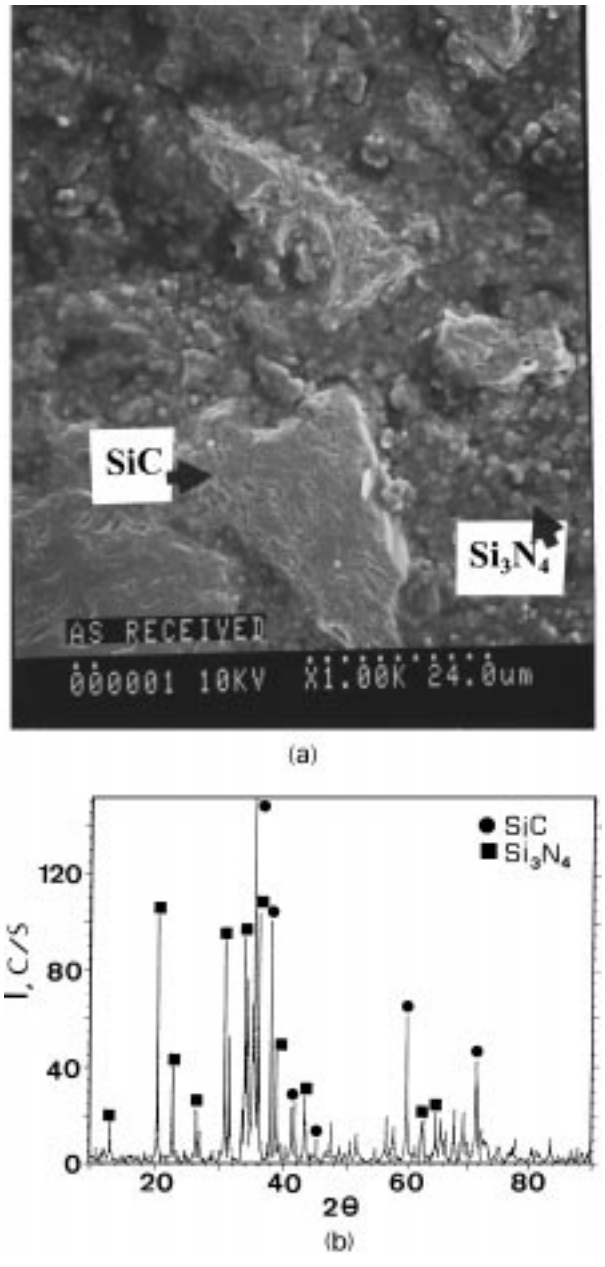

Figure 3 (a) Distribution and morphology of SiC and Si_3N_4 phases in NBSC, and (b) X-ray diffraction peaks of these phases for the NBSC in the as-received condition.

of surface cracks on the SiO_2 into the SiC/Si_3N_4 matrix. Finally, Fig. 8a, b are X-ray diffractograms for the scale development at various temperatures after 1 and 40 hours exposure in air. The absence of diffraction peaks corresponding to Si_3N_4 is probably due to surface irregularities and the presence of the surface oxide scale which did not allow X-rays to reach the Si_3N_4 matrix effectively. Also notice that the SiC peaks, and intensity peaks corresponding to cristobalite and/or tridymite increase in intensity with temperature. From these figures it is apparent that crystallization of the amorphous SiO_2 scale is promoted at all the oxidation temperatures used in this work.

4. Discussion

4.1. Oxidation kinetics

The potential oxidation reactions expected at elevated temperatures in NBSC are:

$$SiC(s) + 3/2O_2(g) \leftrightarrow SiO_2(s) + CO(g) \quad (1a)$$

$$Si_3N_4(s) + (3/4)O_2(g) \leftrightarrow (3/2)Si_2N_2O(s) + (1/2)N_2(g) \quad (1b)$$

$$(3/2)Si_2N_2O(s) + (3/2)O_2(g) \leftrightarrow SiO_2(s) + N_2(g) \quad (1c)$$

All of the above reactions give rise to an overall mass gain. Experimentally, two oxidation stages were found as a direct result of the relatively high porosity present in the NBSC in agreement with Evans *et al*. [8]. During the oxidation stage I, given that the surface interconnected pore network is in contact with the environment, direct reaction of oxygen at both the inner porous regions, as well as the external surfaces, is expected to be dominant. Since the internal surface area provided by the open porosity is much larger than the external one, the oxidation rates in stage I are far superior to those exhibited in stage II. In this work, at 1100 °C a stage corresponding to a single parabolic oxidation mechanism was dominant during the exposure times considered. Apparently, at this relatively low oxidation temperatures most of the oxidation (internal and external) can be associated to a single parabolic scaling limited by molecular oxygen transport across the oxide scale.

At temperatures above 1100 °C, relatively high parabolic oxidation rates were found to precede the second stage of parabolic scale growth. Accordingly, the value of $(\Delta W/A)_a^2$ (see Table III) was used to describe the transition between both stages of parabolic scale growth. Moreover, the mass constants (k_m) consistently increased with temperature (see Fig. 1b). This effect can be attributed to a rapid closure of surface porosity through the development of a continuous SiO_2 scale preventing further internal oxidation. Notice that at the increasing temperatures, the mass gain found just before the external continuous film develops through oxidation consistently decreases at increasing temperatures (Fig. 1b). Apparently, the volume changes associated with the formation of SiO_2 coupled with the increasing rates of oxidation at the higher temperatures effectively fill up the open spaces provided by the pore channels and block the penetration of further oxygen into the internal pores. Although the process is strongly dependent on the pore geometry, size and distribution, once the external pores are closed through oxidation, no internal oxidation is expected. Consequently, it is apparent that at the highest oxidation temperatures the mass gain needed to produce a fully continuous film is significantly reduced.

4.2. Stage II

As a continuous SiO_2 scale develops throughout the external sample surface, oxidation occurs by inward diffusion of oxygen trough the continuous silica phase giving rise to a drastic reduction in the NBSC oxidation rates. Published work [1–4] on the oxidation resistance of monolithic SiC and Si_3N_4 indicate that, at temperatures below 1400 °C, the oxidation rate of SiC is 2-3 orders of magnitude greater than that corresponding to

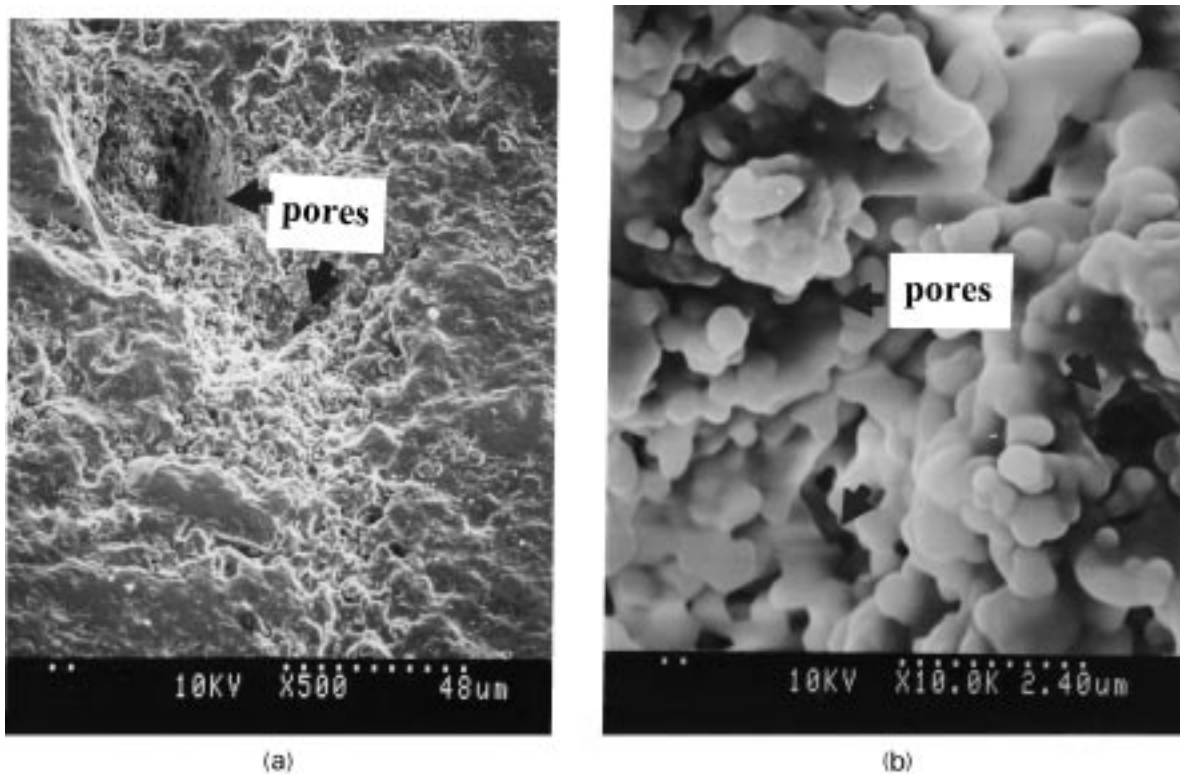

Figure 4 (a) Surface scale after oxidation at 1300°C for one hour in air, and (b) detail of the scale development indicating that the initial NBSC surface is still porous even though a continuous oxide is already present.

Si_3N_4. Accordingly, in the NBSC it is expected that the surface regions covered by SiC particulates will develop a continuous oxide layer before the Si_3N_4 matrix. Furthermore, the formation of an apparent oxide sublayer [1, 3] suggests that the oxidation of Si_3N_4 might be associated with the formation of Si_2N_2O. Although in the present work a subsurface scale phase is found to develop beneath the continuous SiO_2 scale (Fig. 5). X-ray determinations of the scale composition did not provide information on the presence of phases other than SiO_2, Si_3N_4, cristobalite, or tridymite (Fig. 8). Consequently, it was not possible to establish the exact nature of this phase.

According to the literature [1–4], the oxidation rate of Si_3N_4 is rate controlled by diffusion of molecular oxygen through the inner oxide layer (Si_2N_2O) formed between SiO_2 and the Si_3N_4 matrix. Hence, the drastic reduction in oxidation rates exhibited by Si_3N_4 have been attributed to the slow diffusivity of oxidant into the SiO_2-Si_2N_2O scale. In addition, once a continuous scale is formed, it is expected that the overall oxidation rate will be controlled by the relative contributions of each of the phases being oxidized according to

$$\mathrm{d}(\Delta W/A)/\mathrm{d}t = f_{\mathrm{SiC}}\,\mathrm{d}(\Delta W/A)_{\mathrm{SiC}}/\mathrm{d}t + f_{\mathrm{Si3N4}}\mathrm{d}(\Delta W/A)_{\mathrm{Si3N4}}/\mathrm{d}t \quad (2)$$

where f is the relative volume fraction of either SiC or Si_3N_4. The above expression does not consider the contribution of the relative surface areas of each of the present phases. It is implicitly assumed that at this stage the internal oxidation paths are fully sealed and oxidation on the NBSC surface is dominant. In the case of a continuous scale (stage II), assuming that during stage II the oxidation rates of both, SiC and Si_3N_4 are parabolic, the resultant oxidation rate will also be parabolic. Since the oxidation rates of SiC are far greater than those exhibited by Si_3N_4 [1], the oxidation process of NBSC is expected to be dominated by the oxidation of SiC. The outcome of this work shows that during the oxidation stage II an apparent activation energy of 132 kJ/mol is found to be associated with the oxidation process. Activation energies of 120–350 kJ/mol have been reported by various authors [14, 15, 17] to describe the oxidation of SiC at temperatures below 1500 °C. Under these conditions, it is generally believed that inward diffusion of molecular oxygen through the SiO_2 phase is rate limiting. Moreover, the corresponding activation energies reported for the oxidation of Si_3N_4 under similar temperature conditions are of the order of 276–464 kJ/mol [31–33]. In this case molecular oxygen diffusion through the inner and structurally dense Si_2N_2O layer becomes rate limiting. Accordingly, in the present work during stage II oxidation of NBSC, the rate limiting step as inferred from the corresponding activation energy is the molecular oxygen diffusion into the SiO_2 scale.

4.3. Stage I

The mechanisms involved during stage I of oxidation are less clear. The parabolic dependence of $\Delta W/A$ with time suggests that inward oxygen diffusion through a scale developed both, at the external and internal porous regions of the NBSC is rate limiting. In the present work, the first stage of oxidation is relatively short, lasting between 1–10 hours, with the time decreasing

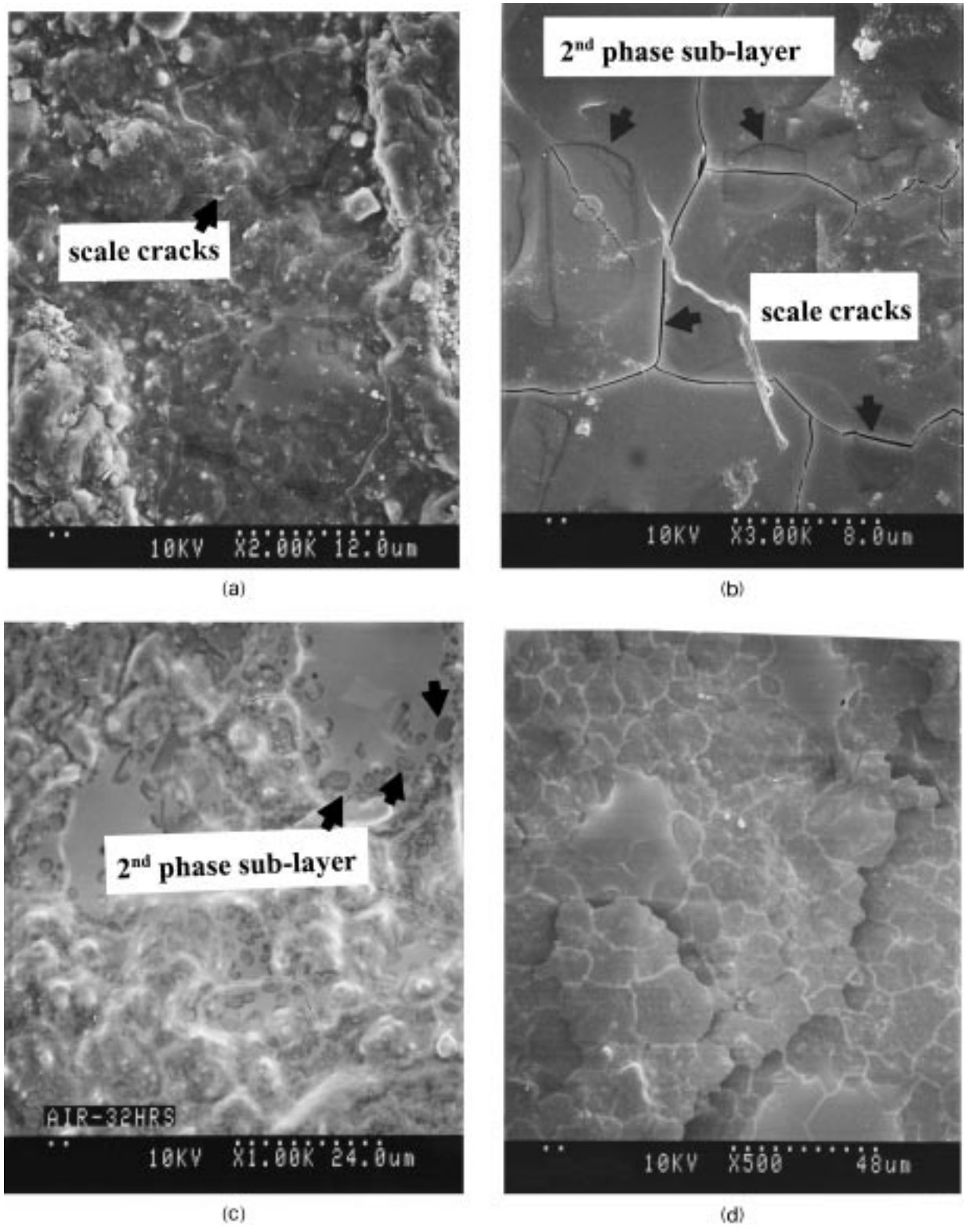

Figure 5 Micrographs showing the development of a continuous oxide scale after air oxidation at (a) 1250°C for 40 h. (b) 1300°C for 32 h. (c) 1340°C for 32 h. and (d) 1400°C for 32 h.

to <1 hour at 1400 °C (see Table III). Moreover, the activation energy in the linear oxidation stage is 55 kJ/mol and does not agree with those corresponding to either a diffusion controlled mechanism [14, 15, 17], or the braking of Si-C or Si-N bonds. Reported bond energies for Si-C are 280 kJ/mol [34] with similar magnitudes expected for Si-N bonds [35]. The apparent activation energy exhibited during this stage does not seem to correspond with the parabolic oxidation mechanism. Possible explanations for the exhibited activation energy are related to; (a) the exhibited mass gain/area through oxidation does not consider the total oxidation area exposed which might be extremely large due to the contribution of the area of the internal pore network; and (b) the development of internal strains in the oxide due to constraints associated with the resultant volume changes as a result of oxidation. Here, the strain effects associated with the resultant volume expansion which arises from internal oxidation, might result in non-parabolic diffusion controlled scale growth [12].

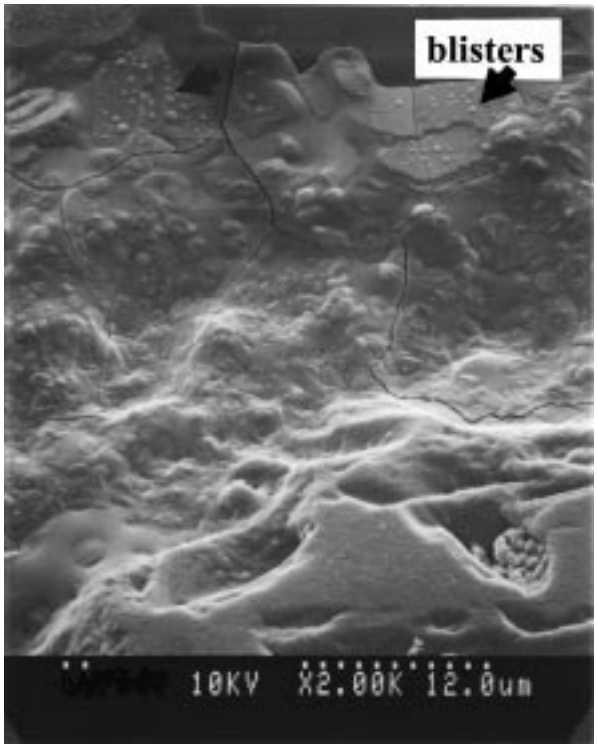

Figure 6 Apparent blisters developed on the surface scale upon oxidation at 1400 °C for 40 h.

Since the rate of oxidation of SiC is expected to be significantly higher than that of Si_3N_4, relatively large internal stresses might develop during oxidation. An estimation of the volume increases ($\Delta V/V$) with f_{SiC} yields values of 0.22 [26, 27]. Hence, the volume changes associated with oxidation of the internal porosity will result in the development of compressive stresses on the pore-surrounding matrix due to accommodation of the resultant oxide. This in turn is expected to effect the oxidation kinetics during this stage. Accordingly, neglecting the volume changes due to Si_3N_4, oxidation, the chemical potential for oxidation under the effect of compressive stresses can be modified according to [28, 29]

$$\Delta\mu = kT \ln\left(P^{*}_{O2}/P^{g}_{O2}\right) - \sigma_c \Delta\Omega \qquad (3)$$

where, $\Delta\mu$ is the chemical potential for oxidation, k is the Boltzman constant, T is the oxidation temperature, P^{*}_{O2} is the equilibrium oxygen pressure at the SiC/SiO_2 interface, P^{g}_{O2} is the oxygen partial pressure in air, σ_c is the compressive internal stress acting on the porous inner oxidized surfaces, and $\Delta\Omega$ is the volume change per oxygen atom in SiO_2. Hence, as an internal oxide forms, strain constraints are built-up which need to be accommodated by the surrounding matrix. This in turn might account for the exhibited behavior during the early oxidation stage. Nevertheless, further studies are needed in order to clearly disclose the active oxidation mechanisms in this stage.

4.4. Thermal stresses

X-ray diffraction indicates that cristobalite and/or tridymite were formed particularly at the highest oxidation temperatures, This in turn lowers the oxidation

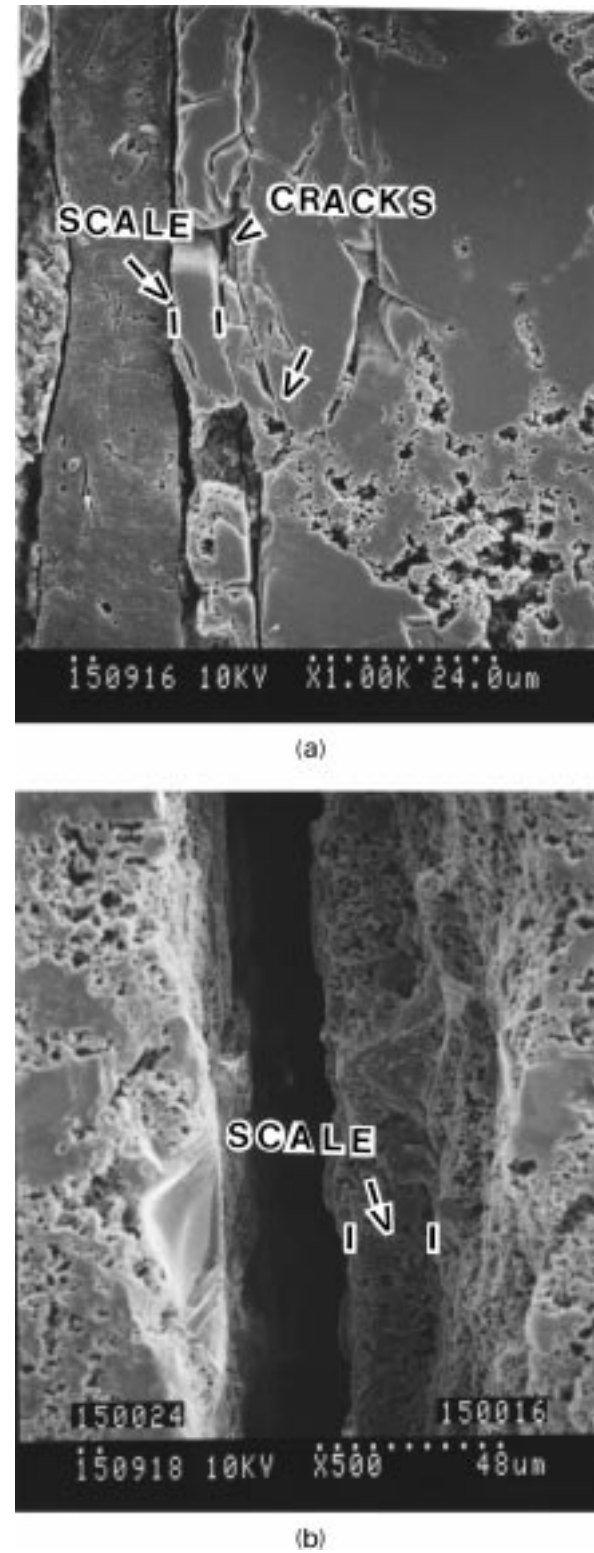

Figure 7 (a) Scale cross-section showing the development and penetration of surface cracks into the NBSC substrate, (b) HF etching to disclose the scale thickness. $T = 1400$°C, for 16 h.

rates as inward oxygen permeation is further hindered. In general, transport in cristobalite is slower than in amorphous SiO_2 [17]. Moreover, the relative differences in the specific volumes of SiO_2, SiC, and Si_3N_4 [34] show that upon transformation of amorphous SiO_2 to cristobalite significant thermal expansion occurs. This in turn might give rise to scale cracking if the scale is not plastic enough to accommodate the local volume differences. In addition, internal stresses might be present as a result of the volume expansion associated

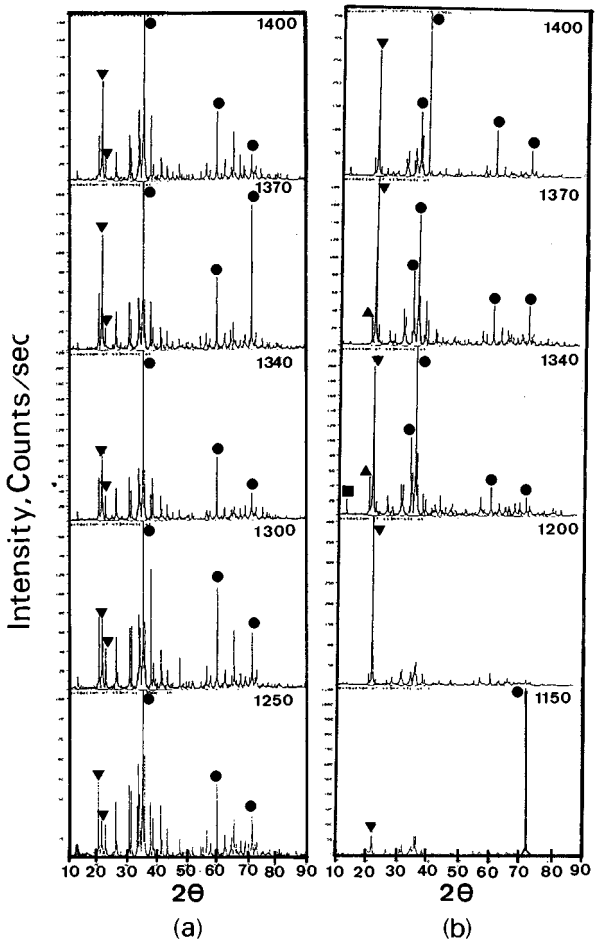

Figure 8 X-ray diffraction patterns after air oxidation at 1150–1400°C for (a) 1 h. and (b) 40 hs. (●= SiC, ■ = Si_3N_4, ▼ = Cristobalite, and ▲ = Tridymite)

with the internal oxidation. Nevertheless, at the oxidation temperatures of interest the scale viscosity is relatively low (as evidenced by the scale blistering (Fig. 6), and the volume increases associated with the external continuous scale can be readily accommodated. Hence, it is unlikely that during the oxidation stage II the observed scale cracking is related to the build up of stress incompatibilities at the elevated temperatures as a result of volume changes. If this were the case, scale cracking should be manifested as a sudden increase in the oxidation rates as a direct oxidation path into the unexposed matrix is generated. Accordingly, any internal/residual stress build-up in the external scale due to the development of β-cristobalite at temperatures above 1100 °C is readily accomodated by viscous flow of the scale. However, at temperatures below 250 °C, there is a relatively large shrinkage ($\approx$1%) due to the β–α cristobalite transformation [36]. At these temperatures the external scale becomes brittle and the stress incompatibilities due to the thermal expansion mismatch of the β–α cristobalite transformation can account for the exhibited crack network found on the external scale surface (Fig. 5). Similar arguments have been suggested to explain the development of crack networks in other oxidized Si_3N_4 ceramics [8, 9]. The interfacial tensile stresses that are expected to build-up at the inner scale/matrix interface as a result of the constraints imposed on the volume of oxide which is forced to occupy the same surface area as the matrix substrate can be estimated by [26, 27].

$$\sigma = E(\Delta V/V)/[1-\nu] \quad (4)$$

where E is Young's modulus, $\Delta V/V$ is the volumetric expansion, and ν is Poisson's ratio. Using the data from Table II for E and ν i.e. values of 16 GPa and 0.25, respectively, and assuming that the strength of the cristobalite scale is roughly 300 MPa [8], the magnitude of $\Delta V/V$ needed to reach fracture is 0.014. This is close to the shrinkage due to the β–α-cristobalite transformation. Hence, increasing the strength of the cristobalite phase will help to reduce the effect of shrinkage stresses on the development of a scale crack network.

The development of surface scale cracks is detrimental to the mechanical strength of the NBSC composite as these cracks can propagate into the matrix material as shown in Fig. 7a. Similar results on the propagation of the scale cracks into the matrix has been reported by Evans *et al*. [8]. If surface cracks can be avoided, the production of SiO_2 through external and internal oxidation is in general beneficial for the composite strength. It has shown that the fracture strength [8] and toughness [6] can be both improved after oxidation. However the arguments are controversial. In general, high temperature oxidation promotes the elimination of impurities through ion migration towards the SiO_2 scale [1, 17] which, in turn is manifest in improved mechanical strength. These benefits can be offset when the oxide layer formed possesses a high concentration of defects [8, 17] such as Co/Fe impurities which are detrimental to the strength of NBSC [7]. Alternatively, the improved strength found after high temperature oxidation has been related to a reduction in potential defects such as flaw sizes and shapes through pore filling and pore rounding as a result of oxidation [8].

Finally, except for the highest oxidation temperatures used in this work, it is not expected that significant evaporation will be dominant [1]. However, at these temperatures, scale evaporation can be induced by the presence of impurities and additives that effectively lower the melting point of SiO_2 such as MgO or Y_2O_3 [17]. Migration of these species to the SiO_2 scale in turn give rise to their corresponding silicates. This effectively lowers the melting point of the oxide scale, and accelerates the oxidation rates [20]. In this work, at 1400°C there were indications of blisters suggesting N_2 and CO bubbling through the scale. Apparently, at these temperatures the scale behaves as a viscous fluid probably through the influence of the additives used (Al_2O_3 and Fe_2O_3, Table I), which are known to lower the melting point of the SiO_2 and to accelerate the oxidation rates [27].

5. Conclusions

A study of the oxidation kinetics of a porous (21.5% porosity) nitride bonded silicon carbide containing 20% SiC in the temperature range of 1100–1400 °C provided the following results.

1. Two oxidation stages were found which corresponded to (I) a rapid parabolic oxidation rate during short term oxidation exposure (0–10 hours), and (ii) second parabolic scale growth stage thereafter.

2. During short term oxidation internal oxidation at pore channels (stage I) was dominant.

3. An experimental activation energy of 55 kJ/mol was obtained during stage I oxidation.

4. After 1–10 hours depending on temperature, surface porosity was sealed by a continuous SiO_2 scale formed. whose growth was parabolic. An activation energy of 132 kJ/mol was associated with this parabolic growth suggesting that inward oxygen diffusion through the SiO_2 scale was rate limiting.

5. The transition between the two stages of parabolic scale growth were related to an apparent mass gain per unit area, $(\Delta W/A)_a$ and time, t_c. In general, $(\Delta W/A)_a$ and t_c consistently decreased as the temperature increased from 1100 to 1400 °C.

6. X-ray diffraction indicated the presence of cristobalite and tridymite, but it was unable to identify a discontinuous phase developed beneath the SiO_2 scale during oxidation.

7. Metallographic observations indicated severe cracking of the scale developed. This was attributed to the relatively large shrinkage (≈1%) associated with the β–α cristobalite transformation occurring at temperatures below 250 °C.

References

1. N. S. JACOBSON, *J. Am. Ceram. Soc.* **76** (1993) 3.
2. H. DU, R. E. TRESSLER, K. E. SPEAR and G. PANTANO, *J. Electrochem. Soc.* **136** (1989) 1527.
3. L. U. J. T. OGBUJI, *J. Am. Ceram. Soc.* **75** (1992) 2995.
4. M. L. TORTI, "Structural Ceramics vol. 29: Treatise on Materials Science and Tech.," edited by J. B. Watchman (Academic Press, 1989) p. 161.
5. H. SAKAI, "Ceramic Transaction," edited by M. D. Scaics, *The Am. Ceram. Soc.* **19** (1991) 741.
6. S. T. BULJAN, J. G. BALDONI and M. L. HUCKABEE, *Ceram. Bull.* **66** (1987) 347.
7. R. LUNDBERG, L. KAHLMAN, R. POMPE, R. CARLSSON and R. WARREN, *ibid.* **66** (1987) 330.
8. A. G. EVANS and R. W. DAVIDGE, *J. Mater. Sci.* **5** (1970) 314.
9. Y. G. GOGOTSI, A. G. GOGOTSI and O. D. SHCHEBINA, *Soviet Powder Metall.* **5** (1986) 40.
10. H. DU, R. E. TRESSLER and K. E. SPEAR, *J. Electrochem. Soc.* **136** (1989) 3210.
11. B. E. DEAL and A. S. GROVE, *J. Appl. Phys.* **36** (1965) 3770.
12. R. H. DOREMUS, "Oxidation of Silicon: Tests of Mechanisms, The Physics and Chemistry of SiO_2 and the Si-SiO_2 interface," edited by C. R. Helms and B. E. Deal (Plenum Press, New York, 1988) p. 17.
13. K. MOTZFELD, *Acta Chem. Scand.* **18** (1964) 1596.
14. T. NARUSHIMA, T. GOTO and T. HIRARI, *J. Amer. Ceram. Soc.* **72** (1989) 1386.
15. Z. ZHENG, R. E. TRESSLER and K. E. SPEAR, *J. Electrochem. Soc.* **137** (1990) 854.
16. K. L. LUTHRA and H. D. PARK, *J. Am. Ceram. Soc.* **73** (1993) 1014.
17. J. A. COSTELLO and R. E. TRESSLER, *ibid.* **69** (1986) 67.
18. *Idem., ibid.* **64** (1981) 327.
19. A. H. HENER, L. U. OGBUJI and T. E. MITCHELL, *ibid.* **63** (1980) 354.
20. S. C. SINGHAL and F. F. LANGE, *ibid.* **58** (1975) 433.
21. W. C. TRIPP and H. C. GRAHAM, *ibid.* **59** (1976) 399.
22. H. CAPPELEN, K. H. JOHANSEN and K. MOTZFELD, *Acta Chem. Scand.* **35** (1981) 247.
23. P. J. JORGENSEN, M. E. WADSWORTH and I. B. CUTLER, *J. Am. Ceram. Soc.* **44** (1961) 258.
24. D. J. CHOI, D. B. FISCHBACH and W. D. SCOTT, *ibid.* **72** (1989) 1118.
25. F. PORZ, G. GRATHWOHL and F. THUMMLER, *Proc. Brit. Ceram. Soc.* **31** (1981) 157.
26. F. PORZ and F. THUMMLER, *J. Mats. Sci.* **19** (1984) 1283.
27. S. C. SINGHAL, *ibid.* **11** (1976) 126.
28. W. DEQING and H. F. LOPEZ, *Mats. Letters* **16** (1993) 313.
29. *Idem., Mats. Sci. and Tech.* **10** (1994) 879.
30. *Idem., J. Eur. Ceram. Soc.* **13** (1994) 203.
31. T. HIRAI, K. NIHARA and T. GOTO, *J. Am. Ceram. Soc.* **63** (1980) 419.
32. W. C. TRIPP and H. C. GRAHAM, *ibid.* **59** (1976) 399.
33. J. SCHLICHTING and L. J. GAUCKLER, *Powder Metall. Intl.* **9** (1977) 36.
34. "Engineering Materials and their Applications," edited by R. A. Flinn and P. K. Trojan (Editorial Houghton Mifflin Co, Boston, 1990) p. 551.
35. "CRC handbook of Chemistry and Physics," 78th ed., edited by D. R. Lide and H. P. R. Frederikse (1997).
36. Y. S. TOULOUKIAN, R. K. KIRBY, R. E. TAYLOR and T. Y. R. LEE, "Thermophysical Properties of Matter" vol. 13 (IFI Plenum, New York, 1970) p. 350, 873, 110.

Received 14 May 1999
and accepted 5 May 2000